AD A091235

14

NSWC/TR-80-208

9 Final rept.,

6

OPTIMAL BODIES FOR MINIMUM TOTAL DRAG AT SUPERSONIC SPEEDS

16 F32392

by

10 NICHOLAS J. MOGA

Strategic Systems Department

17 SF32392594

12 57

11

MAY 1980

NAVAL SURFACE WEAPONS CENTER

Dahlgren, Virginia 22448 Silver Spring, Maryland 20910

411567

80 10 21 12

UNCLASSIFIED

SECURITY CLASSIFICATION OF THIS PAGE (When Data Entered)

REPORT DOCUMENTATION PAGE — READ INSTRUCTIONS BEFORE COMPLETING FORM

1. REPORT NUMBER: NSWC TR-80-208 ✓
2. GOVT ACCESSION NO.: AD-A09 1 235
3. RECIPIENT'S CATALOG NUMBER:
4. TITLE (and Subtitle): OPTIMAL BODIES FOR MINIMUM TOTAL DRAG AT SUPERSONIC SPEEDS
5. TYPE OF REPORT & PERIOD COVERED: Final
6. PERFORMING ORG. REPORT NUMBER:
7. AUTHOR(s): Nicholas J. Moga
8. CONTRACT OR GRANT NUMBER(s):
9. PERFORMING ORGANIZATION NAME AND ADDRESS: Naval Surface Weapons Center (K21) ✓ Dahlgren, VA 22448
10. PROGRAM ELEMENT, PROJECT, TASK AREA & WORK UNIT NUMBERS: SF-32-392-591
11. CONTROLLING OFFICE NAME AND ADDRESS: Naval Sea Systems Command Washington, DC
12. REPORT DATE: May 1980
13. NUMBER OF PAGES: 58
14. MONITORING AGENCY NAME & ADDRESS (if different from Controlling Office):
15. SECURITY CLASS. (of this report):
15a. DECLASSIFICATION/DOWNGRADING SCHEDULE:
16. DISTRIBUTION STATEMENT (of this Report): A. Unlimited Distribution
17. DISTRIBUTION STATEMENT (of the abstract entered in Block 20, if different from Report):

18. SUPPLEMENTARY NOTES:
19. KEY WORDS (Continue on reverse side if necessary and identify by block number):

Minimum Drag
Aerodynamic
Optimal Bodies

20. ABSTRACT (Continue on reverse side if necessary and identify by block number)

Two new methods were developed for predicting projectile shape which yield minimum total drag at supersonic speeds. The first technique is an Eulerian scheme that uses modified Newtonian theory and Prandtl-Meyer expansion for pressure drag with Van Driest skin friction and semi-empirical base drag prediction. The second scheme iterates body coordinates with the second-order shock-expansion theory and the same skin friction and base drag methods to minimize the total drag. A different shape is determined for each length-to-diameter ratio and Mach number

DD FORM 1 JAN 73 1473 EDITION OF 1 NOV 65 IS OBSOLETE

S/N 0102-LF-014-6601

UNCLASSIFIED

SECURITY CLASSIFICATION OF THIS PAGE (When Data Entered)

20. ABSTRACT (Continued)

The first technique was found to calculate a reasonably accurate optimal shape, but did not predict accurate drag coefficients. It was found that the modified Newtonian theory plus Prandtl-Meyer expansion predicted pressure drag coefficients much too low whereas the second-order shock-expansion method gave good results. The second technique predicted both accurate optimal shapes and drag coefficients. Optimal shapes were predicted using the second technique for Mach numbers 2-5 and length-to-diameter ratios of 4, 5, and 6. They were found to compare well with experimental data.

FOREWORD

This study covers work initiated in 1978 to improve an optimization of projectile shape for minimum drag. The work was partially supported by NAVSEA Task Number SF-32-392-591.

This report was reviewed and approved by Dr. Frank G. Moore, Head, Aeromechanics Branch and by Mr. C. A. Fisher, Head, Weapon Dynamics Division.

Released by:

R. T. RYLAND, JR., Head
Strategic Systems Department

RE: Distribution Statement
Unlimited per Ms. Vicki Koehl, NSWC/Dahlgren, Technical Publ. Div.

ABSTRACT

Two new methods were developed for predicting projectile shape which yield minimum total drag at supersonic speeds. The first technique is an Eulerian scheme that uses modified Newtonian theory and Prandtl-Meyer expansion for pressure drag with Van Driest skin friction and semi-empirical base drag prediction. The second scheme iterates body coordinates with the second-order shock-expansion theory and the same skin friction and base drag methods to minimize the total drag. A different shape is determined for each length-to-diameter ratio and Mach number.

The first technique was found to calculate a reasonably accurate optimal shape, but did not predict accurate drag coefficients. It was found that the modified Newtonian theory plus Prandtl-Meyer expansion predicted pressure drag coefficients much too low whereas the second-order shock-expansion method gave good results. The second technique predicted both accurate optimal shapes and drag coefficients. Optimal shapes were predicted using the second technique for Mach numbers 2-5 and length-to-diameter ratios of 4, 5, and 6. They were found to compare well with experimental data.

ACKNOWLEDGEMENT

The author would like to express his appreciation for the guidance and help given by Dr. Fred R. DeJarnette of North Carolina State University. His help in developing the Eulerian Optimization was indespensible and his encouragement was continual. Also thanks are given to Dr. Frank G. Moore and Dr. Charles M. Blackmon of the Naval Surface Weapons Center for their support during this effort.

CONTENTS

FIGURES

INTRODUCTION

The need for optimal body design in minimizing total drag has been generated by the Navy's requirement for projectiles to have longer range, shorter flight times, and higher terminal velocity. The work of Moore[1] in 1959 analyzed optimal projectile shape using mostly empirical techniques. Results of this study indicated that range of current projectiles could be increased by more than fifty percent using aerodynamic design considerations. Because of high experimental costs, it is desired that optimal body shapes be generated by cheaper analytic means. Three main contributers of drag must be predicted in order to evaluate total body drag. They are pressure or wave drag, skin friction, and base drag. The major portion of analytical work has been in the prediction of optimal forebody shapes by minimizing pressure drag. Minimum wave drag shapes were found by von Karman[2], using slender body theory, Cole[3] using Newtonian theory, and Miele[4], who included skin friction drag with pressure drag calculations. The above optimization studies have led to configurations which adequately predicted optimum supersonic nose shapes but neglected base drag contributions. The work of Hager, et. al.[5] attempted to define optimal projectile shape including total drag analytically. However, when compared to experiment, the drag predicted was found to be low.

The object of this effort was to create a more accurate technique of analytically predicting minimized total drag body shapes. The supersonic regime (Mach numbers 2-6) was chosen since projectiles were the bodies of interest. The approach was to first try a different optimization scheme than that of Reference 5 while still using the same drag prediction methodology. A more accurate pressure drag prediction technique was then tried to further improve optimization. A third optimization scheme was finally found that gave more accurate results although it was computationally more time consuming.

FIRST PREDICTION METHOD

An Eulerian optimization scheme was first tried on the drag predictive techniques of Refernce 5. The Eulerian optimization is similar to that of Miele in Reference 4. The drag prediction methodology of Refernce 5 uses modified Newtonian pressure distribution plus Prandtl-Meyer expansion, Van Driest turbulent skin-friction analysis, and a semi-empirical base drag prediction. The total drag coefficient is defined by

$$C_D = \frac{2\pi}{S_r} \int_o^{\ell} C_p(x)\ r\{r'(x)\}\ dx + C_{f_\infty} \frac{S_w}{S_r} - C_{p_B} \left(\frac{d_B}{d_r} \right)^2 \qquad (1)$$

where

$C_p(x)$ is the pressure coefficient predicted by modified Newtonian theory plus Prandtl-Meyer expansion, C_{f_∞} is the flat-plate turbulent skin-friction coefficient, and C_{p_B} is the base pressure coefficient. The forebody pressure coefficient is found using modified Newtonian theory

$$C_p = C_{p_o} \sin^2 \theta \qquad (2)$$

where

C_{p_o} is the stagnation pressure coefficient behind a normal shock defined by

$$C_{p_o} = \frac{2}{\gamma M_\infty^2} \left[\frac{(\gamma + 1) M_\infty^2}{2} \right]^{\frac{\gamma}{\gamma-1}} \left[\frac{\gamma+1}{2\gamma M_\infty^2 - (\gamma-1)} \right]^{\frac{1}{\gamma-1}} - 1 \qquad (3)$$

and θ is the body slope with

$$r'(x) = \tan\theta . \qquad (4)$$

The stagnation pressure calculation is limited from a blunted nose to the point of maximum thickness. At the point of maximum thickness (θ=0), Equation (2) gives $C_p = 0$ leading to small inaccuries.

The afterbody pressure calculation is calculated from the Prandtl-Mayer expansion

$$\frac{dp}{d\theta} = \frac{\gamma p M^2}{M^2-1} . \qquad (5)$$

This expression is limited to negative slopes of less than 8^{o} on the afterbody.

The skin-friction prediction is from Reference 6 which assumes a fully turbulent boundary layer. The mean skin friction coefficient for a flat plate, C_{f_∞} is found through iteration of the following equation

$$\frac{0.242}{A\ (C_{f_\infty})^{1/2}} \quad (Tw/T_\infty)^{-1/2} \quad (\sin^{-1} C_1 + \sin^{-1} C_2) =$$

$$\log_{10} (Re_\infty\, C_{f_\infty}) - \frac{1+2n}{2} \log_{10} (Tw/T_\infty) \qquad (6)$$

where

$$A = \left[\frac{(\gamma - 1)\ M_\infty^2}{2\ T_w/\ T_\infty} \right]^{1/2} ; \quad B = \frac{1 + (\gamma-1)}{2\ M_\infty^2\ \ T_w/T_\infty} - 1 ;$$

$$C_1 = \frac{2\ A^2 - B}{(B^2 + 4A^2)^{1/2}} ; \quad C_2 = \frac{B}{(B^2 + 4A^2)} .$$

The variable n in Equation (6) is the power in the power viscosity law

$$\frac{\mu}{\mu_\infty} = \left[\frac{T_w}{T_\infty}\right]^n \tag{7}$$

and for air n is 0.76. A Prandtl number of unity and a zero pressure gradient in the fully developed turbulent boundary layer are assumed in the relations above. The freestream Reynolds number is

$$Re_\infty = \frac{\rho_\infty V_\infty \ell}{\mu_\infty} \tag{8}$$

where

ℓ is the total configuration length. The temperature ratio T_w/T_∞ is found assuming an adiabatic wall and by introducing the turbulent recovery factor R_T.

$$\frac{T_w}{T_\infty} = 1 + R_T \frac{\gamma-1}{2} M_\infty^2 \; . \tag{9}$$

The turbulent recovery factor varies approximately as the cube root of the Prandtl number so that

$$R_T = \sqrt[3]{Pr} \; . \tag{10}$$

To compensate for the assumption of Pr=1 in the Van Driest method, the actual Prandtl number of air, Pr=0.73 was used in Equation (10). Thus Equation (9) becomes

$$\frac{T_w}{T_\infty} = 1 + 0.9 \frac{\gamma-1}{2} M_\infty^2 \; . \tag{11}$$

One can now combine Equations (8) and (11) with (6) to solve for C_{f_∞}. The Newton-Raphson method is used to calculate C_{f_∞} in Equation (6).

The base drag is calculated using a semi-emperical technique developed by Moore[7]. A mean curve of experimental base pressure data is given in Figure 1. This data assumes a fully developed turbulent boundary layer ahead of a long cylindrical afterbody. The effect of a boatail significantly alters base pressure and must be accounted for. The empirical equation used is

$$C_{D_B} = -C_{p_B} \left(\frac{d_B}{d_r}\right)^2 = -C_{p_{BA}} \left(\frac{d_B}{d_r}\right)^3 \quad . \qquad (12)$$

Equation (12) can be used for all Mach numbers where $C_{p_{BA}}$ is the base pressure given in Figure 1.

EULERIAN OPTIMIZATION

FOREBODY

The predictive techniques described above were then used with an Eulerian optimization scheme.[4] Hager used an algorithm based on LaGrange duality theory for convex control problems in his analysis and it was thought the Eulerian technique might be a more accurate optimization scheme. DeJarnette, in an unpublished work, developed the technique below and found it simpler than that of Hager, et al.

The total drag equation was redefined as

$$C_D\, r_{max}^2 = 2\int_{x_i}^{x_c}\left(C_{p,nose}\, r' + C_f\right) r\, dx + 2\int_{x_c}^{x_f}\left(C_{p,aft}\, r' + C_f\right) r\, dx + C_{p_o} r_i^2 - C_{p_{AB}} \frac{r_f^3}{r_c} \tag{13}$$

with the r and x coordinates defined in Figure 2.

Now let

$$F = \left[C_p\, r' + C_f\sqrt{r'^2 + 1}\right] \tag{14}$$

noting

$$r' = \frac{dr}{dx} \tag{15}$$

and

$$F = F(r, r'). \tag{16}$$

The type of body being optimized is of the general configuration shown in Figure 2. It consists of a blunted nose, and boatail with a discontinuity at the corner. A maximum body radius and length to diameter ratio (L/D) are constraints. Using (14), (15), and (16) consider the first variation of equation (13) as

$$\delta\left(\frac{C_D r_{max}^2}{2}\right) = \int_{x_i}^{x_{c-}} \left(F_r - \frac{dF_{r'}}{dx}\right)\tilde{\delta} r dx + \int_{x_{c+}}^{x_f} \left(Fr - \frac{d}{dx} Fr'\right)\tilde{\delta} r dx +$$

$$\left[(F - r'F_{r'})\ \delta x + F_{r'}\delta r\right]_i^f - \left[\Delta(F - r'F_{r'})\delta x + \Delta F_{r'}\delta r\right] +$$

$$C_{Po}\ r_i\ \delta r_i - \frac{3}{2} C_{P_{AB}} \frac{r_f^2}{r_c} \delta r_f \tag{17}$$

where

the subscripts C− and C+ denote conditions immediately before and after the corner at x_c and $\tilde{\delta} r$ represents the distance between the external and comparison arc as defined in Reference 4. For minimum drag, the variation of drag in equation (17) equals zero so now consider the right side of the equation as distinct parts.

For the integrand of the integrals in Equation (17) to be zero,

$$F_r - \frac{d}{dx}(Fr') = 0 \tag{18}$$

but since F is a function of r and r', then from Miele[4]

$$F - r'Fr' = \text{constant} = -C_o. \tag{19}$$

Recalling that

$$F = C_p r' + C_f \sqrt{r'^2 + 1}\ ,$$

$$C_p = C_p(r')$$

and

$$F_{r'} = \left[r \frac{d(C_p r')}{dr'} + \frac{C_f r'}{\sqrt{r'^2 + 1}} \right] .$$

Then,

$$F - r'F_{r'} = \left[C_p r' + C_f \sqrt{r'^2 + 1} \right] r - r' r \left[C_p + r' \frac{dC_p}{dr'} \right] -$$

$$\frac{r r'^2 C_f}{\sqrt{r'^2 + 1}} = r \left[\frac{C_f}{\sqrt{r'^2 + 1}} - r'^2 \frac{dC_p}{dr'} \right] \tag{20}$$

and further

$$r \left[r'^2 \frac{dC_p}{dr'} - \frac{C_f}{\sqrt{r'^2 + 1}} \right] = \text{constant} = C_o \; . \tag{21}$$

This equation holds for the forebody and afterbody.

At the corner of the body, $\delta r = 0$ but $\delta x \neq 0$, which means the value of the maximum thickness is fixed, but its x location is not fixed. This condition gives

$$\Delta(F - r'Fr') = 0 \tag{22}$$

and therefore

$$(C_o)_{forebody} = (C_o)_{afterbody} \tag{23}$$

At the beginning of the forebody (the subscript i location in Figure 2), $\delta x = 0$ and $\delta r \neq 0$. This gives

$$-F_{r'} + C_{Po} r_i = 0 \tag{24}$$

For the forebody, using Modified Newtonian theory, Equation (2) yields

$$C_p = C_{Po} \frac{r'^2}{1 + r'^2} \tag{25}$$

and

$$\frac{d}{dr'} (C_p r') = C_{Po} \frac{r'^2(3 + r'^2)}{(1 + r'^2)^2} \; . \tag{26}$$

Now use equation (21) at the i location and find

$$\frac{-r_i' (3 + r_i'^2)}{(1 + r_i'^2)^2} + 1 - \frac{C_f}{C_{Po}} \frac{r_i'}{\sqrt{1 + r_i'^2}} = 0 \tag{27}$$

Using a Newton-Raphson technique, equation (27) can be solved for the optimum initial slope, r_i'.

Using the Modified Newtonian pressure distribution, it follows that

$$\frac{dC_p}{dr'} = C_{Po} \left[\frac{(1 + r'^2)\, 2r' - r'^2\, 2r'}{(1 + r'^2)^2} \right] = \frac{2C_{Po}\, r'}{(1 + r'^2)^2} \; . \tag{28}$$

For the forebody, equation (21) gives

$$r \frac{2C_{p_o} r'^3}{(1 + r'^2)^2} - \frac{C_f}{\sqrt{r'^2 + 1}} = C_o \tag{29}$$

or rearranging

$$\frac{r}{C_o} = \frac{(1 + r'^2)^2}{2C_{p_o} r'^3 - C_f (1 + r'^2)^{3/2}} \ . \tag{30}$$

Now on the forebody section x can be related to r by

$$dx = \frac{dr}{r'} = \frac{dr}{dr'} \ \frac{dr'}{r'} \ . \tag{31}$$

Applying this result to equation (30), it follows that

$$\frac{1}{C_o} \ \frac{dr}{dr'} = \frac{2C_{p_o} r'^2 \ (1 + r'^2) \ (r'^2 - 3)}{\left[2C_{p_o} r'^3 - C_f \ (1 + r'^2)^{3/2}\right]^2} \ . \tag{32}$$

Using the function x/C_o for x in equation (31) it follows that

$$d\left(\frac{x}{C_o}\right) = \frac{2C_{p_o} r'(1 + r'^2)(r'^2 - 3)dr'}{\left(2C_{p_o} r'^3 - C_f(1 + r'^2)^{3/2}\right)^2} \ . \tag{33}$$

Equations (30) and (33) give two parametric equations to determine the optimum forebody shape.

AFTERBODY

The afterbody shape optimization starts with the base condition, $\delta x = 0$, but $\delta r \neq 0$ from equations (17) and (18)

$$F_{r'} - \frac{3}{2} C_{p_{AB}} \frac{r_f^2}{r_c} = 0 \tag{34}$$

and

$$F_r' = r\frac{d(C_p r')}{dr'} + \frac{C_f r'}{\sqrt{r'^2+1}} = r\left(C_p + r'\frac{dC_p}{dr'}\right) + \frac{C_f r'}{\sqrt{r'^2+1}} \,. \quad (35)$$

Combining

$$r\left(C_p + r_f'\frac{dC_p}{dr'}\right)_f - \frac{3}{2}C_{p_{AB}}\frac{r_f^2}{r_C} + \frac{C_f r_f'}{\sqrt{r_f'^2+1}} = 0 \quad (36)$$

and rearranging, the condition to be satisfied at the base is:

$$\left(C_p\right)_f + r_f'\frac{dC_p}{dr'} + \frac{C_f r_f'}{\sqrt{r_f'^2+1}} = \frac{3}{2}C_{p_{AB}}\frac{r_f}{r_C} \quad . \quad (37)$$

Use the Prandtl-Meyer Function to determine the pressure on the afterbody as follows

$$r' = \tan\theta \quad (4)$$

$$\theta = -\nu + K_o \quad (38)$$

where

ν is the Prandtl-Meyer function and K_o is a constant evaluated at the corner. The first integral of the Euler equation is given by

$$r\left(r'^2\frac{dC_p}{dr'} - \frac{C_f}{\sqrt{r'^2+1}}\right) = C_o \quad . \quad (39)$$

The pressure coefficient is defined by

$$C_p = \frac{p - p_\infty}{q_\infty} = \frac{p_\infty}{q_\infty}\left(\frac{p}{p_o}\frac{p_o}{p_\infty}\right) - 1 \quad . \quad (40)$$

Differentiating equation (40) by r'

$$\frac{dC_p}{dr'} = \frac{p_o}{q_\infty} \frac{d}{dr'} \left(\frac{p}{p_o}\right) = \frac{p_o}{q_\infty} \frac{d}{dM^2} \left(\frac{p}{p_o}\right) \frac{dM^2}{d\theta} \frac{d\theta}{dr'} \quad . \tag{41}$$

Noting that

$$\frac{dr'}{d\theta} = \frac{1}{\cos^2\theta}$$

$$\frac{p}{p_o} = \left(1 + \frac{\gamma - 1}{2} M^2\right)^{\frac{-\gamma}{\gamma - 1}}$$

and

$$\frac{dC_p}{d\theta} = \frac{p_o}{p_\infty} \frac{\gamma \frac{p}{p_o} M^2}{\sqrt{M^2 - 1}}$$

from compressible aerodynamic theory[3] subtitition into equation (41) yields

$$\frac{dC_p}{dr'} = \frac{dC_p}{d\theta} \frac{d\theta}{dr'} = \frac{p_o \gamma}{q_\infty} \frac{\frac{p}{p_o} M^2}{\sqrt{M^2 - 1}} \cos^2\theta \quad . \tag{42}$$

Now substituting in equation (38) the optimal equation for r on the afterbody is as follows

$$r\left(\frac{p_o}{q_\infty} \gamma \frac{\frac{p}{p_o} M^2 \sin^2\theta}{\sqrt{M^2 - 1}} - \frac{C_f}{\sqrt{r'^2 + 1}}\right) = C_o \quad . \tag{43}$$

Let the bracketed quantity in equation (43) be called g(r'), then

$$r = \frac{C_o}{g(r')}$$

and

$$\frac{dr}{dr'} = \frac{-C_o}{g^2} g' .$$

Then

$$dx = \frac{dr}{r'} = \frac{-C_o \, g' dr'}{g^2 r'}$$

or

$$d\left(\frac{x}{C_o}\right) = \frac{-g' dr}{g^2 r'} \tag{44}$$

Integrating by parts from the corner ($x=x_C$), equation (44) becomes

$$\frac{x - x_C}{C_o} = \frac{r}{C_o r'} - \frac{r_C}{C_o r'_C} + \int_{x_C}^{x} \frac{r}{C_o} \frac{dr'}{r'^2} \tag{45}$$

where

$$\frac{r}{C_o} = \frac{1}{g} = \frac{1}{\left(\frac{p_o}{q_\infty} \frac{\gamma \frac{p}{p_o} M^2 \sin^2\theta}{\sqrt{M^2 - 1}} - \frac{C_f}{\sqrt{r'^2 + 1}}\right)} . \tag{46}$$

If the integration variable is changed to M^2, the Prandtl-Meyer expression is

$$d\theta = \frac{-\sqrt{M^2 - 1}\, d(M^2)}{2M^2(1 + \frac{\gamma-1}{2} M^2)}$$

then

$$dr' = \frac{d\theta}{\cos^2\theta} = \frac{-\sqrt{M^2 - 1}\, d(M^2)}{2M^2\left(1 + \frac{\gamma-1}{2} M^2\right)}$$

and the expression for x on the afterbody is

$$\frac{x - x_C}{C_o} = \frac{r}{C_o r'} - \frac{r_C}{C_o r'_C} - \int_{M_C^2}^{M^2} \frac{r}{C_o} \frac{\sqrt{M^2 - 1}\; d(M^2)}{2\sin^2\theta\; M^2\left(1 + \frac{\gamma-1}{2} M^2\right)} \quad . \quad (47)$$

The Prandtl-Meyer function is defined as[8]

$$\nu = \sqrt{\frac{\gamma + 1}{\gamma - 1}}\; \tan^{-1}\sqrt{\frac{(\gamma - 1)(M^2 - 1)}{\gamma + 1}} - \tan^{-1}\sqrt{M^2 - 1} \quad . \quad (48)$$

For comparision with Reference 5, $p = p_\infty$ should be true at $\theta = 0$. The Mach number when $\theta = 0$, M_R, is defined by

$$\frac{p_\infty}{p_o} = \left(1 + \frac{\gamma - 1}{2} M_R^2\right)^{\frac{-\gamma}{\gamma-1}}$$

or (49)

$$M_R^2 = \frac{2}{\gamma - 1}\left(\left(\frac{p_\infty}{p_o}\right)^{\frac{-(\gamma-1)}{\gamma}} - 1\right)$$

with p_o being the stagnation pressure aft of the normal shock. It should be noted that M_R is not necessarily the same as M_C. Recalling equation (38)

$$\theta = -\nu + K_o \quad (38)$$

$$K_o = \nu_{(M=M_R)}$$

and

$$\nu = K_o - \theta$$

for θ less than zero on the afterbody.

The calculation on the afterbody starts at the corner with an assumed θ. Equation (45) is integrated with M greater than M_c until the base is reached where equation (37) is satisfied. At each integration step the pressure coefficient is defined as

$$C_p = \frac{p_o}{q_\infty}\left(\frac{p}{p_o}\frac{p_o}{p_\infty} - 1\right) \tag{50}$$

and therefore

$$C_{p_o} = \frac{p_o - p_\infty}{q_\infty} = \frac{p_o}{q_\infty} - \frac{2}{\gamma M_\infty^2}$$

or

$$\frac{p_o}{q_\infty} = \left(C_{p_o} + \frac{2}{\gamma M_\infty^2}\right) \quad . \tag{51}$$

Dividing both sides of equation (51)

$$\frac{(p_o/q_\infty)}{C_{p_o}} = 1 + \frac{2}{\gamma M_\infty^2 \, C_{p_o}}$$

A better constant can be defined by replacing C_o with

$$C_1 = \frac{C_o}{C_{p_o}} \quad .$$

The equations for the forebody using Modified Newtonian pressure theory are

$$\frac{r}{C_1} = \frac{(1+r'^2)^2}{\left(2r'^3 - \frac{C_f}{C_{p_o}}(1+r'^2)^{3/2}\right)} \tag{52}$$

$$d\left[\frac{x}{C_1}\right] = \frac{2r'(1 + r'^2)(r'^2 - 3)\, dr'}{\left[2r'^3 - \frac{C_f}{C_{p_o}}(1 + r'^2)^{3/2}\right]^2} \tag{53}$$

On the afterbody using the Prandtl-Meyer expansion for the pressure coefficient, the equations are

$$\frac{r}{C_1} = \left[\left(1 + \frac{2}{\gamma M_\infty^2 C_{p_o}}\right) \frac{\frac{\frac{P}{P_o}}{\gamma} M^2 \sin^2\theta}{M^2 - 1} - \frac{C_f}{C_{p_o}\sqrt{r'^2 + 1}}\right]^{-1} \tag{54}$$

$$\frac{X - X_c}{C_1} = \frac{r}{C_1 r'} - \frac{r_c}{C_1 r'_c} - \int_{M_c^2}^{M^2} \frac{r}{C_1} \frac{\sqrt{M^2 - 1}\, d(M^2)}{2\sin^2\theta M^2\left(1 + \frac{\gamma-1}{2}M^2\right)} \tag{55}$$

where

$$\theta = K_o - \nu.$$

EULERIAN RESULTS

Equations (52) through (55) were digitized in a marching scheme to optimize a projectile shape given Mach number and initial conditions. The initial slope was found using equation (27) which started the marching scheme. Transition from forebody to afterbody was made at the maximum diameter location. The end location (position x_f in Figure 2) was determined by minimization of base drag effects.

Cases of Mach numbers 2 and 3 with sea level conditions were run and compared to that of Reference 5. Plots of these cases are shown in Figure 3. In the Mach 3 case, the Eulerian Optimization gave drag coefficients which were approximately 10% less than the method of Reference 5. This does not compare well with the experimental data of Reference 9 for the Navy 25 mm round. The wind tunnel data in Reference 9 was for a shape optimized on a L/D ratio of 5 with maximum diameter at 3.5 calibers (x_c/x_f = .7) at Mach 3. The code used in Reference 5 predicted a drag coefficient 22% less than experiment while the Eulerian optimization was 31% less. The Mach 2 case is much worse although it should be noted that the wind tunnel model was optimized for Mach 3. A comparison of the predicted optimum shape for L/D = 5, Mach = 3 is given is Figure 4. Both shapes are very similar to that used in Reference 9.

The shapes generated by Eulerian optimization were similar to those generated in Reference 5 for different maximum diameter location. The Eulerian scheme did not predict the drag more accurately which was the goal. This led one to question the accuracy of the optimization although the shape generated was essentially the same as previous attempts. The failing of the drag prediction to be accurate was attributable mostly to the wave drag prediction of the modified Newtonian theory. The better accuracy of second-order shock-expansion was then given consideration.

OPTIMIZATION USING SECOND-ORDER SHOCK-EXPANSION PREDICTION

EULERIAN TECHNIQUE

The second-order shock-expansion theory was used by Syvertson and Dennis in Reference 10 to predict wave drag for pointed bodies at angle-of-attack equal to zero. The method was modified by Jackson et. al. in Reference 11 to account for blunted bodies. The body in this method is replaced by a tangent body which is a series of conical frustrums tangent to the actual body at various body locations. An attempt was made to use the Eulerian optimization scheme with the second-order shock-expansion method as the wave drag component. The Newtonian theory was optimized using a first-order scheme from Reference 4. A second-order scheme also from Reference 4 was initiated, but was rejected due to complexity of the terms and type of scheme needed for numerical integration of the shock-expansion theory. Of major concern was the large size of required matrix operations. A less complex minimization scheme, using the second-order shock-expansion method for the surface pressures, was developed and is described below.

SECOND-ORDER SHOCK-EXPANSION PREDICTION METHOD

The new optimization scheme developed here is essentially a geometric iteration method of determining an optimum shape. The accurate second-order shock-expansion technique developed in Reference 12 was chosen to replace the modified Newtonian plus Prandtl-Meyer expansion because of its relatively quick computation time and extensive use in body alone aerodynamics. The Mach number range is from 1.5 to 6.0 in this method.

The original second-order shock-expansion method was developed for pointed noses with attached shock waves.[3] In the basic method, pressure on the initial cone is obtained from a cone solution and is considered constant on the cone. The pressure drop at the first juncture is calculated from standard Prandtl-Meyer expansion. The pressure along the next frustrum varies exponentially and is made to satisfy three boundary conditions. The first boundary condition is that the pressure (p_2) just after the corner of the initial cone and first conical frustrum is obtained from Prandtl-Meyer expansion. The second boundary condition is that the pressure gradient $(\partial p/\partial s)_2$ at this position (just after the corner) is obtained from an approximate expression developed in Reference 10. The third boundary condition is defined by setting the pressure at infinity equal to the cone pressure (p_c) that would exist on the first conical frustrum if it were infinitely long. The pressure along a conical frustrum can then be given by[12]

$$p = p_c - (p_c - p_2)\, e^{-n} \tag{56}$$

where

$$n = \left[\frac{\partial p}{\partial s}\right]_2 \frac{(x - x_2)}{(p_c - p_2)\cos\delta_2} \quad (\text{for } n > 0) \tag{57}$$

The cone angle δ_2 is defined as the conical frustrum inclination. The Pressure gradient just downstream of the corner (position 2) is determined from the approximate expression[10]

$$\left(\frac{\partial p}{\partial s}\right)_2 - \lambda_2 \left(\frac{\partial \delta}{\partial s}\right)_2 = \frac{B_2}{r}\left(\frac{\Omega_1}{\Omega_2}\sin\delta_1 - \sin\delta_2\right) + \frac{B_2}{B_1}\frac{\Omega_1}{\Omega_2}\left[\left(\frac{\partial p}{\partial s}\right)_1 - \lambda_1\left(\frac{\partial \delta}{\partial s}\right)_1\right] \tag{58}$$

where

$$B = \frac{\gamma p M^2}{2(M^2-1)} \tag{59}$$

$$\lambda = \frac{2\gamma p}{\sin 2\mu} \tag{60}$$

$$\Omega = \frac{1}{M}\left[\frac{1+\frac{(\gamma-1)}{2}M^2}{\left(\frac{\gamma+1}{2}\right)}\right]^{\frac{(\gamma+1)}{2(\gamma-1)}} \tag{61}$$

In the above equations $(-\partial\delta/\partial s)$ is the curvature of the surface which is zero on conical frustrums, Ω is the one dimensional area ratio, and the subscript i refers to the position just before the corner. Since the pressure is constant on the initial cone $(\partial p/\partial s)$ equals zero on the first conical frustrum after the initial cone. For all subsequent conical frustrums the pressure gradient is obtained from the derivative of Equation (56). For more details of this method, see Reference (10).

The original second-order shock-expansion was modified by Jackson, et. al.[11] for blunt bodies by using the modified Newtonian pressure distribution up to a "matching point". The matching point was set as the maximum angle for an attached shock wave. Beyond the matching point, the original second-order shock-expansion is used. DeJarnette and Jones[12] made two modifications to that of Reference 11 that increased accuracy. A computer code was developed using these modifications along with the Van Driest[6] skin-friction prediction and the semi-empirical base pressure method devised by Moore[7].

The modifications made in Reference 12 consist of introducing an "exact" pressure gradient downstream of a corner and determining a new matching point for matching second-order shock-expansion with modified Newtonian theory on blunt-nose bodies. The "exact" pressure gradient is based on the method of characteristics. The following equations were derived on the surface streamline[12]

$$\frac{\partial}{\partial \delta}\left[Q + \frac{\Omega \sin \delta}{r}\right] = -\left(\frac{\gamma+1}{4}\right) \frac{M^4 Q}{(M^2 - 1)^{3/2}} \tag{62}$$

where

$$Q = \left(\frac{\Omega}{B}\right) \left[\frac{\partial p}{\partial s} - \lambda \frac{\partial \delta}{\partial s}\right] \tag{63}$$

Equation (62) is integrated numerically around the corner along with the Prandtl-Meyer expansion to determine Q. Equation (63) is solved for the pressure gradient ($\partial p/\partial s$). A new matching point was found to be the position on the nose where the modified Newtonian pressure distribution gives a local Mach number of 1.15.

NEW OPTIMIZATION METHOD

The new optimization method starts with a semi-optimum shape. An iteration method is then used to determine the body coordinates which minimizes the total drag using the modified second-order shock-expansion method to calculate surface pressures along with the Van Driest skin-friction and empirical base drag methods.

The selection of a semi-optimum body began with a review of the optimum studies of Reference 1 through 5 and 9. The general conclusions of the first five references indicated that a 2/3 or 3/4 power law forebody gave minimum drag. References 5 and 9 further found that a good after body would be one with a conical boatail. Further, Reference 9 noted that for practical applications, a blunted nose is necessary. A review of experimental data of optimum shapes confirmed the theory that one optimizes for a given Mach number. An arbitrary selection was made from the results of the above study that the semi-optimum shape would be chosen for Mach 3. The initial bluntness was made L/D dependent from the results of the Eulerian Optimization. The forebody was set as a 3/4 power law body allowing for the selection of different maximum diameter positions. From the maximum diameter location aft a 6° conic was chosen. The resulting semi-optimum body differed from Reference 5 and the Eulerian Optimization in the forebody shape and the boatail cutoff location. A total of 20 coordinates were selected as an adequate description of the body with 14 on the forebody and the remaining 6 on the boatail.

A set of independent coordinates $\{ x_i \}_{i=1}^{20}$ were selected with the i=14 point taken as the point of maximum diameter (note i in this section represents a coordinate). The corresponding set of dependent variables $\{ r_i \}_{i=1}^{20}$ were initially determined from the semi-optimum body. For prescribed values of $\{x_i\}$, r_{14}, M_∞, and Reynolds number, the drag coefficient can be represented by

$$C_D = C_D(r_i) \qquad i = 1,2,\ldots,20 \; (i \neq 14)$$

It is desired to determine the values of r_i which makes C_D a relative minimum. If $\{r_{i,o}\}$ represents the initial set, or a set from a previous iteration, then the Taylor series expansion gives*

$$C_D = C_{D_o} + \sum_{n=1}^{\infty} \frac{1}{n!} \left\{ \left[\sum_i (\Delta r_i \frac{\partial}{\partial r_i}) \right]^n C_D \right\}_o \tag{64}$$

and thus:

$$\frac{\partial C_D}{\partial r_i} = \left(\frac{\partial C_D}{\partial r_i}\right)_o + \sum_j \left(\frac{\partial^2 C_D}{\partial r_i\, \partial r_j}\right)_o \Delta r_j + \cdots \quad . \tag{65}$$

For Δr_j sufficiently small the higher order terms may be neglected. A necessary condition for a relative minimum for C_D is

$$\frac{\partial C_D}{\partial r_i} = 0 \quad .$$

Thus Equation (65) gives

$$0 = \left(\frac{\partial C_D}{\partial r_i}\right)_o + \sum_j \left(\frac{\partial^2 C_D}{\partial r_i\, \partial r_j}\right)_o \Delta r_j \quad . \tag{66}$$

Equation (66) represents a linear system of equations for the unknowns Δr_j. However, it is cumbersome to calculate the cross derivatives

$$\frac{\partial^2 C_D}{\partial r_i\, \partial r_j} \qquad \text{for } i \neq j.$$

Therefore, Equation (66) is approximated by

$$0 = \left(\frac{\partial C_D}{\partial r_i}\right)_o + \left(\frac{\partial C_D}{\partial r_i^2}\right)_o \Delta r_i \quad . \tag{67}$$

---

*in all the analysis here i=14 is suppressed.

The derivatives in Equation (67) are formed by the following central difference quotients

$$\left(\frac{\partial C_D}{\partial r_i}\right)_o \doteq \frac{C_{D_i}^{+} - C_{D_i}^{-}}{2\Delta r_i} \tag{68}$$

$$\left(\frac{\partial^2 C_D}{\partial r_i^2}\right)_o \doteq \frac{C_{D_i}^{+} - 2\, C_{D_o} + C_{D_i}^{-}}{(\Delta r_i)^2} \tag{69}$$

where

$$\left.\begin{aligned} C_{D_i}^{+} &= C_D(r_{j,o},\ r_{i,o} + \delta r_i) \\ C_{D_i}^{-} &= C_D(r_{j,o},\ r_{i,o} - \delta r_i) \end{aligned}\right\}\quad j = 1,2,\ldots,20;\ j \neq i$$

and δr_i is two percent of r_i.

The iteration process involves calculating C_{D_o}, $C_{D_i}^{+}$ and $C_{D_i}^{-}$ (i = 1,...,20). Then using equations (68) and (69), equation (67) can be used to calculate Δr_i. Then new values of r_i are calculated by adding Δr_i to the old values. The iteration process is continued until convergence which was assumed to occur when Δr_i changed less than one percent. In the iteration process, if $|\Delta r_i| > \delta r_i$ then the magnitude of Δr_i was taken to be Δr_i. Again, note that r_i for i=14 was not changed since it is the maximum diameter point.

Convergence did not occur in cases where the maximum diameter location was less than 25% of the total length. This is probably due to the negligence of the cross product terms.

RESULTS

The optimization scheme described above was digitized in an efficient manner to minimize computation time. Since the maximum diameter location is an input parameter, cases were run varying this location (x_c/x_f). Also varied were Mach number and total length to diameter ratios. Results of typical runs for sea level conditions are given in Figures 5, 6, and 7. As a comparison, the shape generated by the new optimization technique is drawn with that of Reference 5 in Figure 8. This shape also is very close to the shape generated by the Eulerian technique (Figure 4). The predicted drag, however, is different. The Mach 3, L/D equal 5 case is found in Figure 9. The Mach 3 Experiment point is that found in the wind tunnel test of Reference 9. The 25 mm shape tested is quite similar to those in Figure 8 with the exception of grooves placed on the boatail. These grooves are used for rotating band attachment and could be responsible for some of the 9.6% difference in drag coefficient. The shapes for other cases using the new scheme compared similarly for other Mach numbers, that is good shape agreement, but different drag coefficients. An interesting development in this method is that the design curves produced are flatter in the optimum drag area than those of Reference 5. This would tend to give projectile designers more freedom in actual shape variation and still produce low drag results. A summary of the Mach 3 cases are shown in Figure 10. These curves indicate the trend of increased x_c/x_f with decrease of L/D for optimum drag. Figures 5, 6, and 7 illustrate the trend of increase in x_c/x_f with increase in design Mach number.

The new optimization iteration code is simple to operate and gives the user ease in running multiple cases. The number of iterations to convergence ranged from 4 to 17. An average case (1 Mach number and L/D) cost approximately $10 on both the IBM 370 and CDC 6700. Core requirements are minimal and the code could be put on larger mini-computers (64K bytes). Output includes the number of iterations to convergence, components of drag, total drag coefficient, and the minimum drag shape coordinates.

CONCLUSIONS AND RECOMMENDATIONS

1. Two numerical methods were developed for calculating optimum projectile shape for minimum total drag.

2. The Eulerian optimization technique calculates similar shapes for minimum drag, but is inaccurate in its prediction of total drag.

3. The new optimization technique gives both an optimum shape and a more accurate drag prediction when compared to experiment.

4. A limitation of the new optimization code is that the maximum diameter location must be greater than 25% of the total length.

5. The ratio of maximum diameter location to total length tends to increase for decreasing L/D ratio and increase with increasing Mach number for optimum shapes.

6. A good agreement between three different predictive techniques lends credibility to the actual shape of minimum drag rounds.

7. This technology should be proved experimentally in both large caliber rounds (such as 76 mm) as well as small caliber rounds.

REFERENCES

1. F. G. Moore, "Study to Optimize the Aeroballistic Design of Naval Projectiles," NWL TR-2337, Dahlgren, VA, September 1969.

2. T. von Karman and N. B. Moore, "Resistance of Slender Bodies Moving with Supersonic Velocities, with Special Reference to Projectiles," APM-54-27.

3. J. D. Cole, "Newtonian Flow Theory for Slender Bodies," U. S. Air Force, Project RAND, RM 1633, 1959.

4. A. Miele, Theory of Optimum Aerodynamic Shapes, The Acadamic Press: New York, 1965.

5. W. W. Hager, F. R. DeJarnette, and F. G. Moore, "Optimal Projectile Shapes for Minimum Total Drag," NSWC TR-3597, Dahlgren, VA, May 1977.

6. E. R. Van Driest, "Turbulent Boundary Layer in Compressible Fluids," JAS, VOL. 18, NO. 3, 1951, pp. 145-160.

7. F. G. Moore, "Body Alone Aerodynamics of Guided and Unguided Projectiles at Subsonic, Transonic, and Supersonic Mach Numbers," NWL TR-2796, Dahlgren, VA, November 1972.

8. A. H. Shapiro, The Dynamics and Thermodynamics of Compressible Fluid Flow, Vol. I, The Ronald Press Company, New York, 1953.

9. L. A. Mason, "Theoretical and Experimental Results for 25 mm and 30 mm Optimum and Low-Drag Projectile Shapes," NSWC TR-79-18, Dahlgren, VA, June, 1979.

10. C. A. Syvertson and D. H. Dennis, "A Second-Order Shock-Expansion Method Applicable to Bodies of Revolution Near Zero Lift," NACA Report 1328, 1957.

11. C. M. Jackson, Jr., W. C. Sawyer, and R. S. Smith, "A Method for Determining Surface Pressure on BLunt Bodies of Revolution at Small Angles of Attack in Supersonic Flow," NASA TN D-4865, 1968.

12. F. R. DeJarnette and K. M. Jones, "Development of a Computer Program to Calculate Aerodynamic Characteristics of Bodies and Wing Body Combinations," NSWC/DL TR-3829, Dahlgren, VA, April 1978.

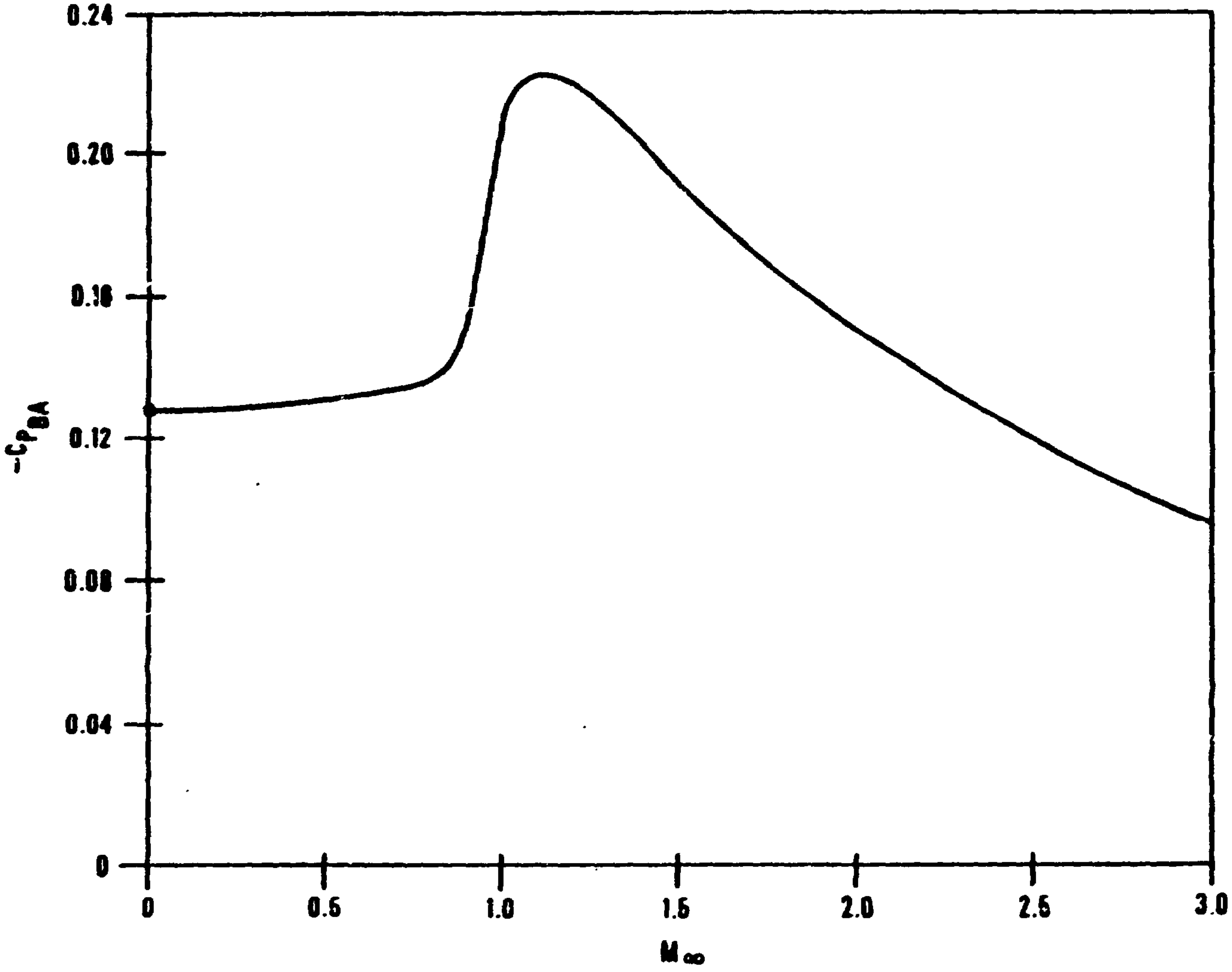

Figure 1. Mean Base Pressure Coefficient

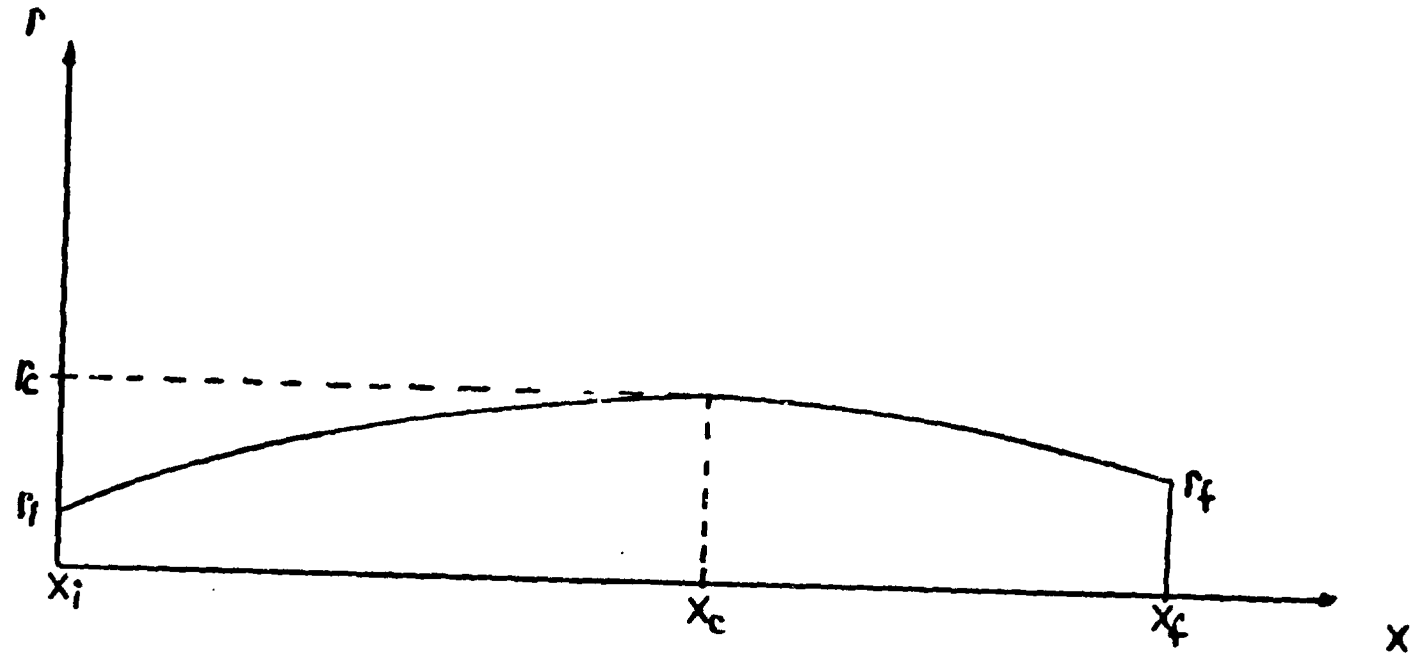

Figure 2. Projectile Coordinates

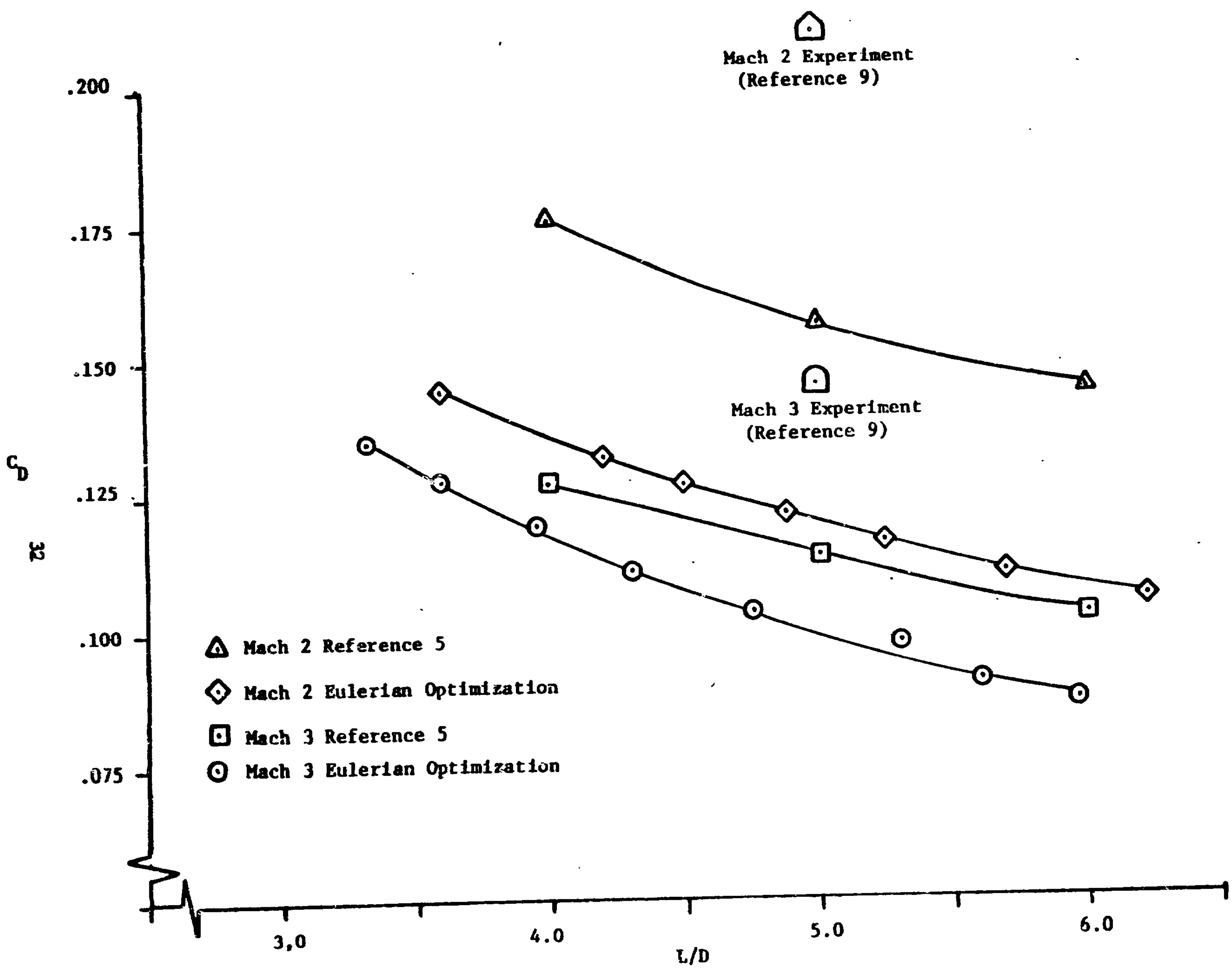

Figure 3. Comparison of Drag Coefficient vs L/D for

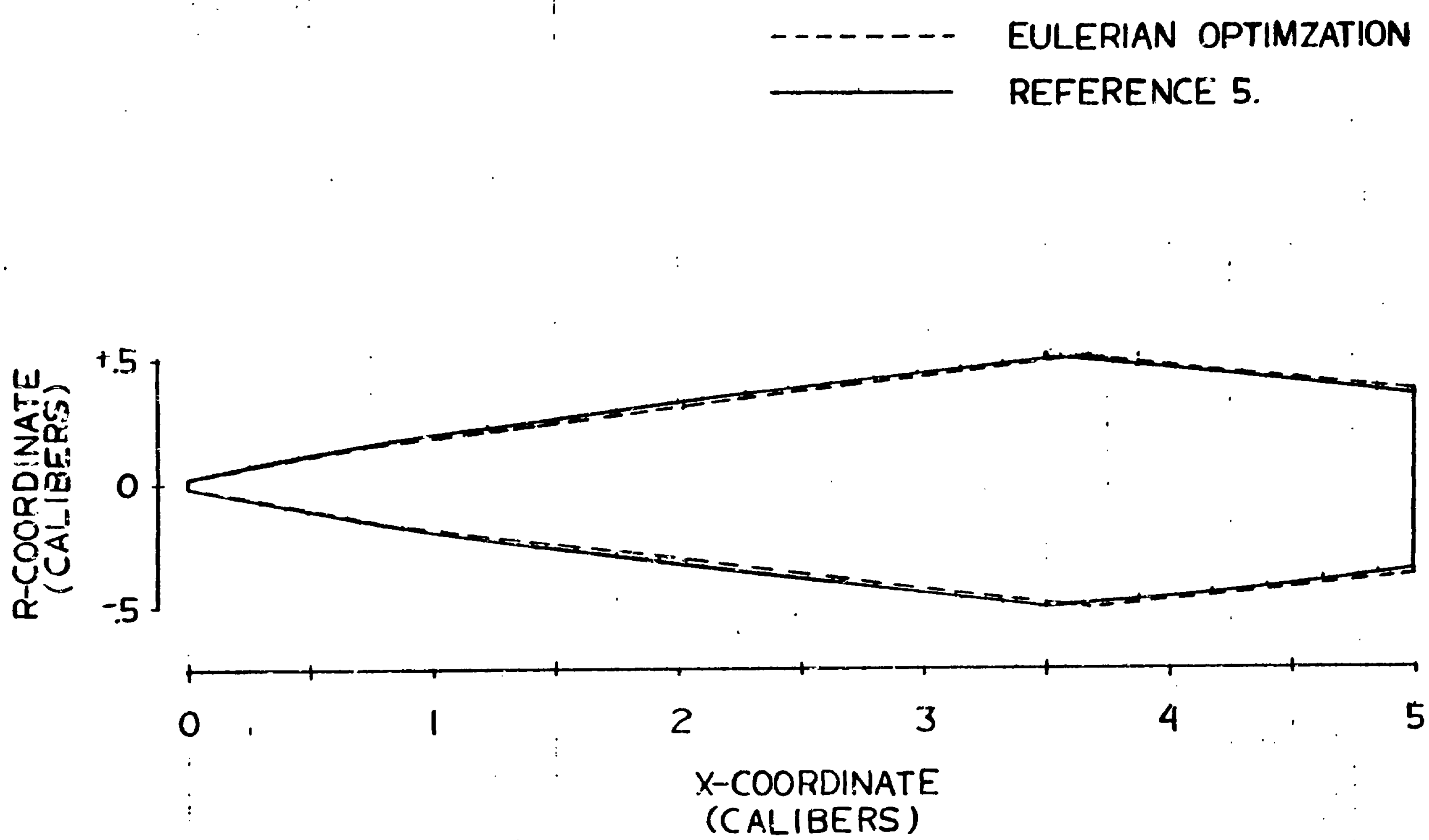

FIGURE 4. OPTIMUM SHAPE COMPARISON, EULERIAN OPTIMIZATION AND REFERENCE 5. MACH NO. = 3, $L/D = 5$

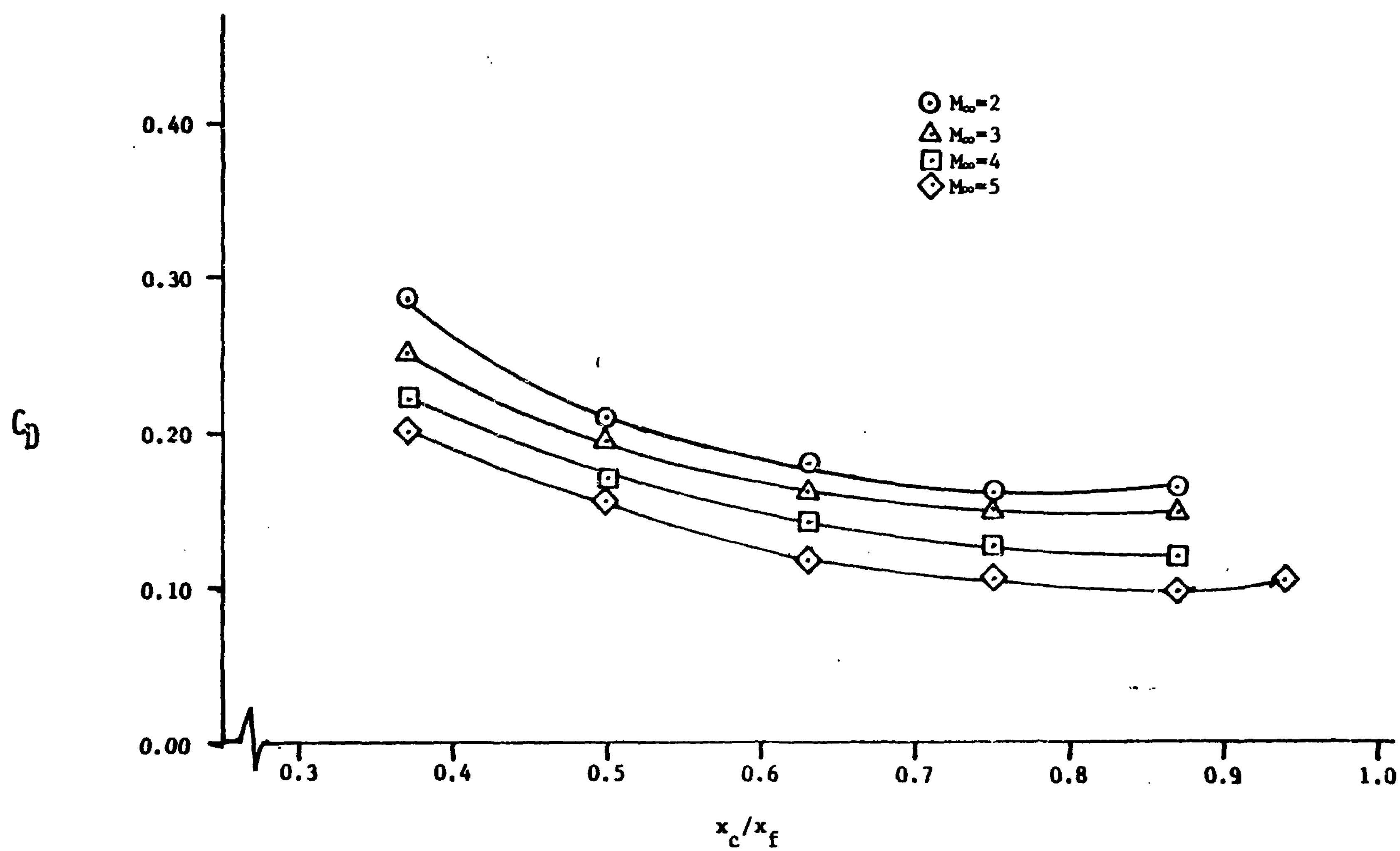

Figure 5. Drag coefficient vs x_c/x_f for L/D=4, New Optimization

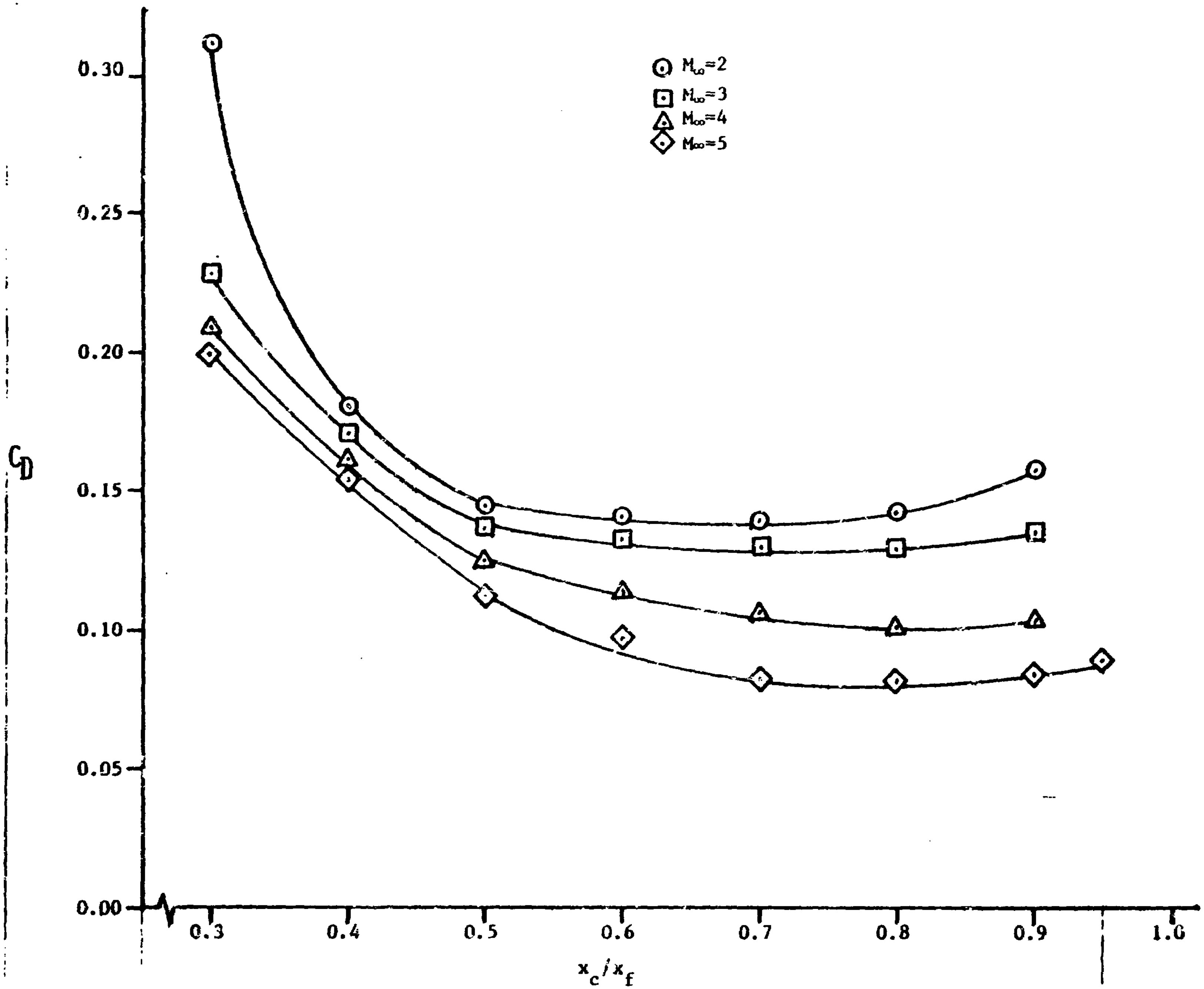

Figure 6. Drag coefficient vs x_c/x_f for L/D=5, New Optimization

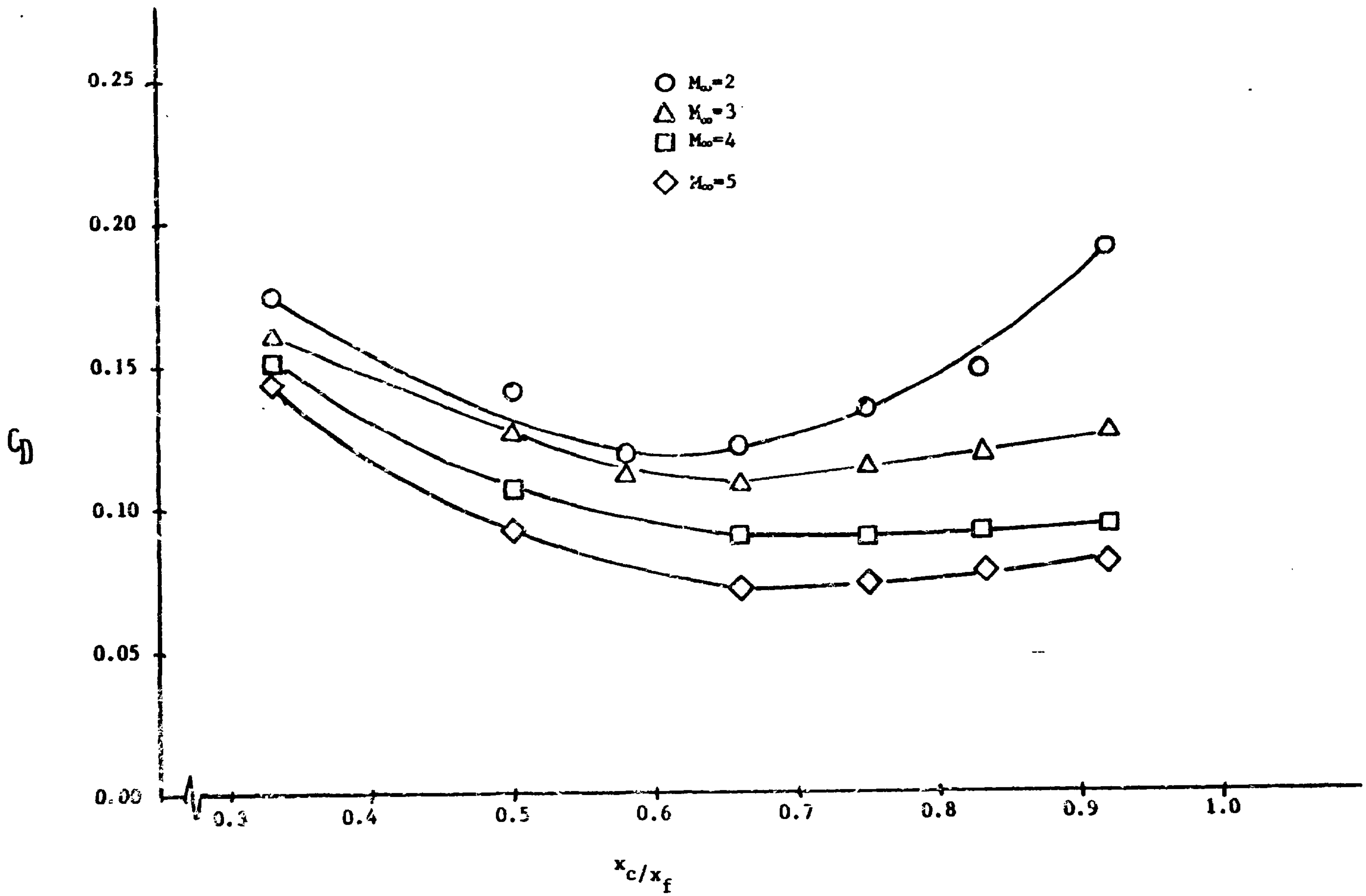

Figure 7. Drag Coefficient vs x_c/x_f for L/D=6, New Optimization

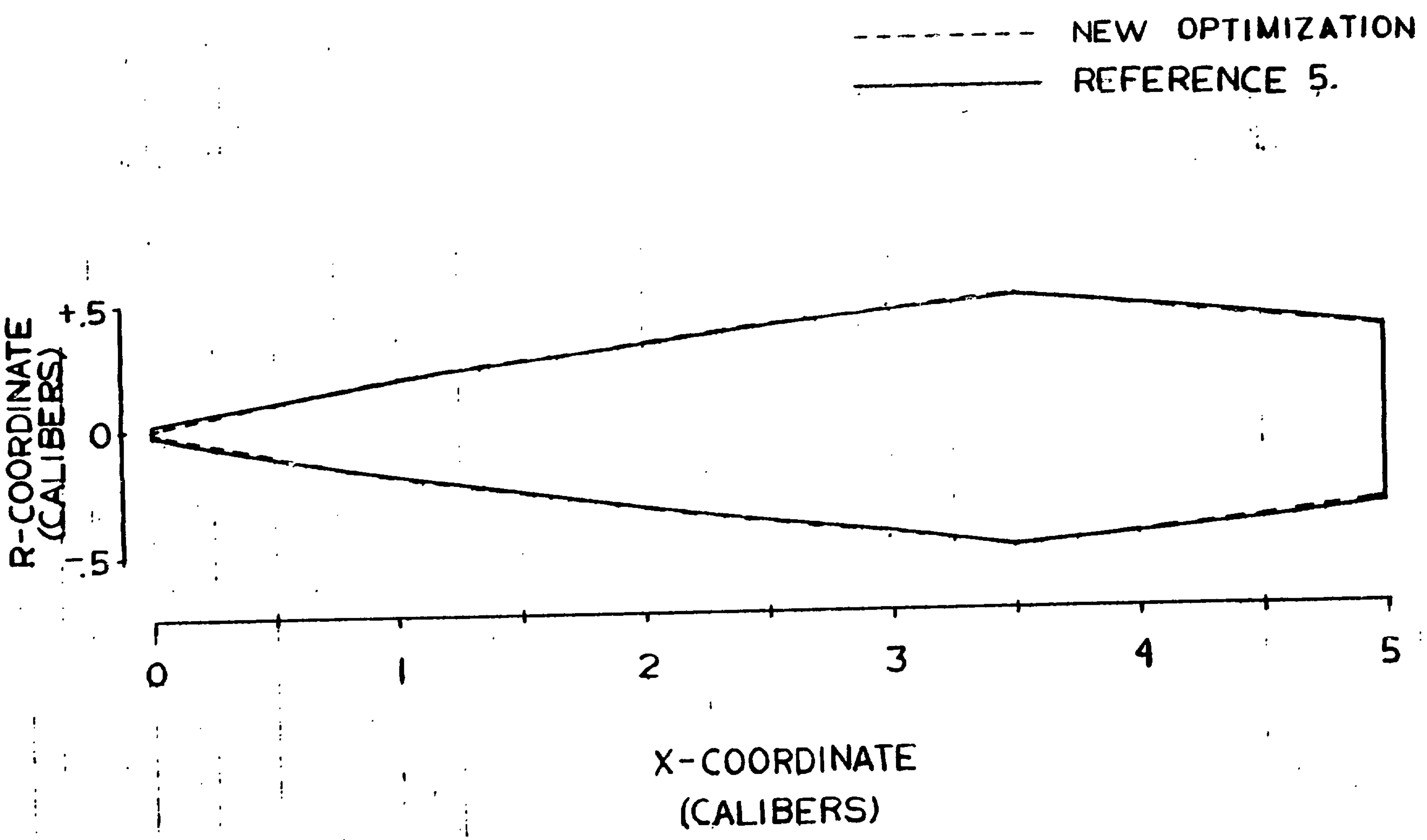

FIGURE 8. OPTIMAL BODY SHAPE FOR MACH NO.=3, X_c/X_f=.7, L/D=5. NEW OPTIMIZATION AND REFERENCE 5.

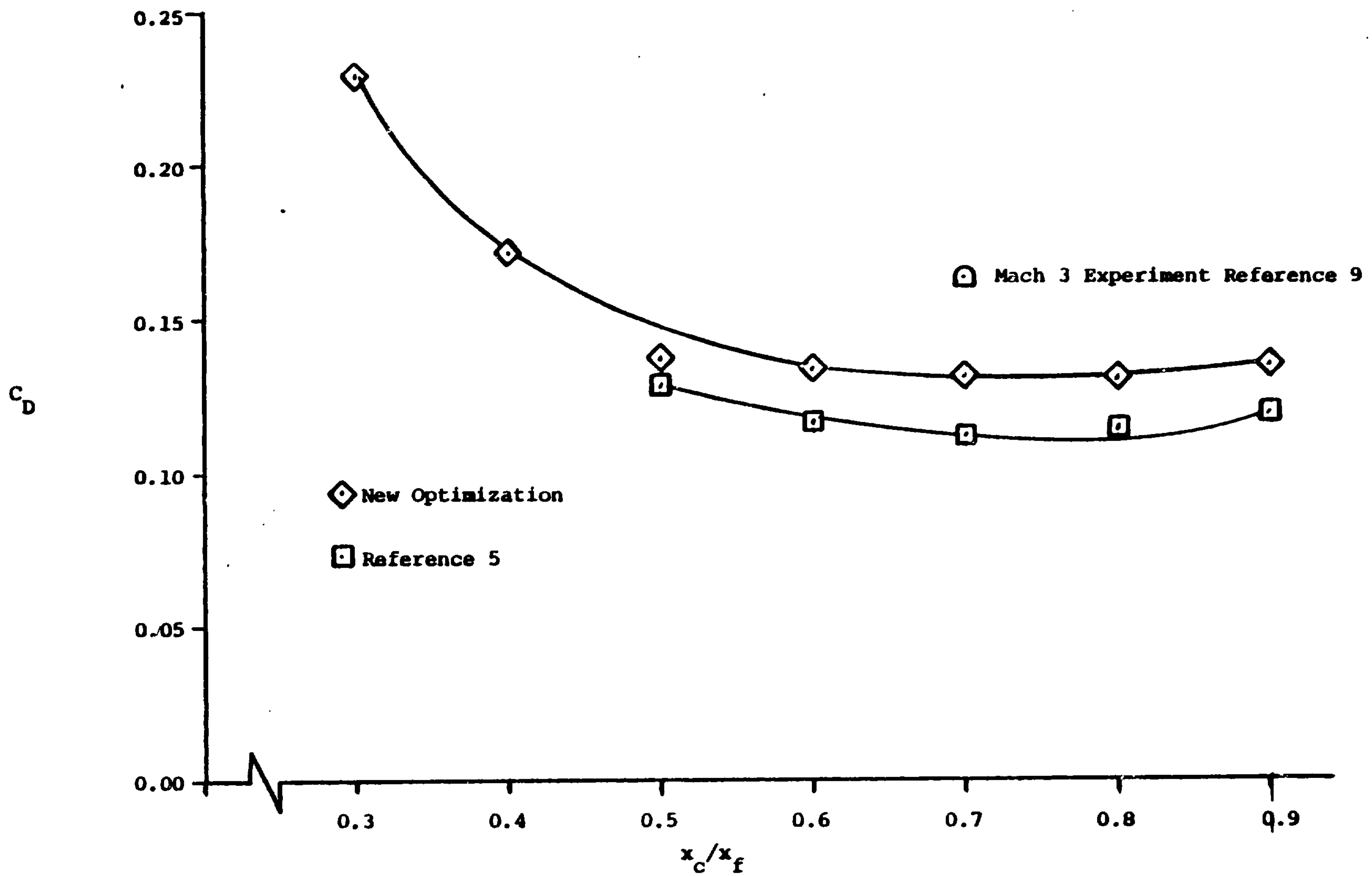

Figure 9. Comparison of Drag Coefficient vs x_c/x_f for Mach No.=3, L/D=5, New Optimization and Reference 5

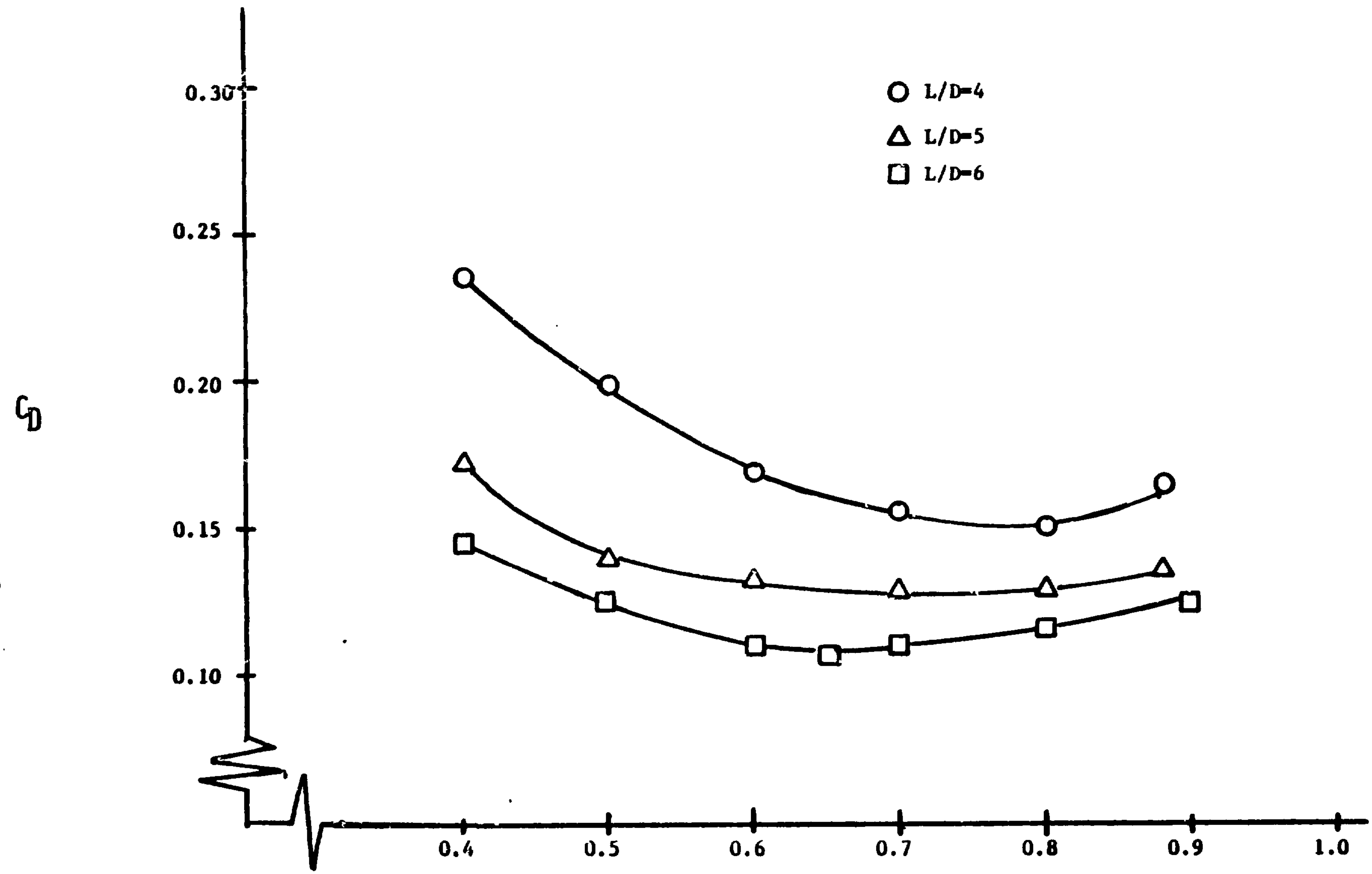

Figure 10. Drag Coefficient vs x_c/x_f, Mach No.=3, New Optimization

GLOSSARY

C_D	drag coefficient
C_{DB}	base drag coefficient
C_f	skin friction coefficient
$C_{f\infty}$	mean skin friction coefficient
Cp	pressure coefficient
Cp_{AB}	base pressure coefficient
D, d	diameter
d_r	reference diameter
ℓ, L	length of configuration
M	Mach number
p	pressure
Pr	Frandtl number
q	dynamic pressure
r	radius of body (Figure 2)
r'	body slope, dr/dx
Re	Reynolds number
R_T	turbulent recovery factor
Sr	reference area
Sw	wetted surface area
T	temperature
Tw	wall temperature
V	velocity
x	length coordinate (Figure 2)
γ	ratio of specific heats
θ	angle along body surface ($\tan^{-1}(dr/dx)$)

μ	coefficient of absolute viscosity
ν	Prandtl-Meyer function
ρ	density of air
Ω	ratio of cross-sectional area of streamtube to that at M=1

Subscripts

0	stagnation condition
1	condition immediately before a corner
2	condition immediately after a corner
B	base conditions
c	position of maximum diameter (Figure 2)
f	position at end of body (Figure 2)
i	position at front of body (Figure 2)
∞	freestream conditions

DISTRIBUTION

Assistant Secretary of the Navy (R&D)
The Pentagon
Washington, DC 20350
ATTN: Technical Library

Center for Naval Analysis
Department of the Navy
Washington, DC 20350
ATTN: Technical Library

Chief of Naval Material
Department of the Navy
Washington, DC 20350
ATTN: Technical Library

Chief of Navy Operations
The Pentagon
Washington, DC 23050
ATTN: Technical Library

Deputy Chief of Naval Operations (Development)
The Pentagon
Washington, DC 23050
ATTN: Technical Library (2)

Chief of Naval Research
Department of the Navy
Washington, DC 20360
ATTN: Technical Library (2)

Office of Chief of Research and Development
Washington, DC 20310
ATTN: Major R. A. Burns
Technical Library

Commanding Officer, Naval Missile Center
Point Mugu, CA 93042
ATTN: Mr. J. Rom
Technical Library

Office of Naval Research
The Pentagon
Washington, DC 23050
ATTN: Dr. R. J. Lundegard
Mr. D. Seigel
Dr. B. Whitehead
Mr. M. Cooper
Mr. R. Cooper
Technical Library

Commander, Naval Material Command
Washington, DC 20362
ATTN: Technical Library

Commander, Naval Sea Systems Command
Washington, DC 20360
ATTN: Mr. L. Pasiuk (SEA-62R)
Technical Library

Commander, Naval Air Systems Command
Washington, DC 20360
ATTN: Mr. W. Volz (AIR-320C)
Technical Library

Commander, Naval Weapons Center
China Lake, CA 93555
ATTN: Dr. L. Smith (Code 3205)
Technical Library

Commander, Naval Ship Research and Development Center
Washington, DC 20007
ATTN: Dr. T. C. Tai
Technical Library

Commanding Officer and Director
Naval Ship Research and Development Center
Carderock, MD
ATTN: Technical Library (2)

Commanding Officer
Naval Air Development Center
Warminster, PA 18974
ATTN: Mr. W. Langen (Code 01A)
Technical Library

Commanding Officer
Naval Ordnance Station
Indianhead, MD 20640
ATTN: Technical Library

Commanding General, U.S. Army Armament Research and Development Command
Dover, NJ 07801
ATTN: Mr. W. Gadomski (DRDAR-SCA-CA) (10)
Mr. A. Loeb
Technical Library (2)

DISTRIBUTION (Continued)

Commanding General, Ballistic Research Laboratory
U.S. Army Test and Evaluation Command
Aberdeen Proving Ground, MD 21005
ATTN: Mr. C. H. Murphy
Mr. A. Platou
Mr. B. McCoy
Mr. L. McAllister
Mr. M. Piddington
Technical Library (2)

Commanding General, Aberdeen Proving Ground
U.S. Army Test and Evaluation Command
Aberdeen Proving Ground, MD 21005
ATTN: Mr. B. Seigal

Commanding General, Edgewood Arsenal
U.S. Army Test and Evaluation Command
Aberdeen Proving Ground, MD 21010
ATTN: Mr. A. Flatou (DRDAR-ACW)
Technical Library (3)

Commanding General, Rock Island Arsenal
U.S. Army Armament Research and Development Command
Rock Island, IL 61201
ATTN: Technical Library (2)

Department of the Army
Office, Chief of Research Development and Acquisition
Washington, DC 20310
ATTN: DAMA-CB
Technical Library

Department of the Army
Office, Assistant Chief of Staff for Force Development
Washington, DC 20310
ATTN: CNNU

Aeronautical Systems Division
USAF
Wright-Patterson AF Base
Dayton, OH 45433
ATTN: Technical Library (2)

Flight Research Center
Edwards AF Base, CA 93523
ATTN: Technical Library

Commanding Officer, Air Force Weapons Laboratory
USAF
Kirtland AF Base, NM 87117
ATTN: Technical Library

DISTRIBUTION (Continued)

General Electric Company
Armament Department
Room 1412
Lakeside Avenue
Burlington, VT 05401
ATTN: Mr. R. H. Whyte

Sandia Laboratories
P.O. Box 5800
Albuquerque, NM 87115
ATTN: Aerodynamics Department
Mr. H. Vaughn
Mr. A. Hodapp

Honeywell, Inc.
Defense Systems Division
600 Second St., NE
Hopkins, MN 55343
ATTN: Mr. R. Aske

North Carolina State University
Department of Mechanical and Aerospace Engineering
Box 5246
Raleigh, NC 27607
ATTN: Prof. F. R. DeJarnette
Technical Library

NASA
Washington, DC 20546
ATTN: Technical Library

Marine Corps Liaison Officer
Field Artillery Board
Fort Sill, OK 73503
ATTN: Technical Library (2)
ATSF-CD
ATZR-BD

Headquarters, USAF
Washington, DC 20330
ATTN: Technical Library

USAF Office of Scientific Research
Washington, DC 20330
ATTN: Technical Library

Headquarters, USAF Systems Command
Andrews AF Base, MD 20331
ATTN: Technical Library

DISTRIBUTION (Continued)

AFATL
Eglin Air Force Base, FL 32542
ATTN: Col. G. D'Arcy (DLD)
Mr. D. Davis (DLD)
Mr. K. Cobb
Mr. G. Winchenbach
Lt. G. Galanos
Mr. J. Jenus
Mr. L. Burge
Lt. Col. Jones
Dr. D. Daniel
Mr. E. Sears
Technical Library (2)

Arnold Engineering Development Center
USAF
Tullahoma, TN 37389
ATTN: Mr. J. Usselton
Technical Library (2)

Aeronautical Research Laboratory
Wright-Patterson AF Base
Dayton, OH 45433
ATTN: Technical Library (2)

Commander
U.S. Army Material Development and Readiness Command
Research and Development Directorate
5001 Eisenhower Avenue
Alexandria, VA 22333
ATTN: DARCOM-SI-AT
DRCDMA - ST

Commander/Director
Chemical Systems Laboratory
USA ARRADCOM
Aberdeen Proving Ground, MD 21010
ATTN: Technical Library

Director
U.S. Army Advanced Material Concepts Agency
2461 Eisenhower Avenue
Alexandria, VA 22314

Commanding General, U.S. Army Missile Command
Redstone Arsenal, AL 35809
ATTN: Mr. R. Deep (DRDMI-PDK)
Technical Library (2)

DISTRIBUTION (Continued)

Commanding General
U.S. Army Material Command AMCD-TP
Washington, DC 20315
ATTN: Mr. J. M. Hughes
Technical Library

Commanding General
Yuma Proving Ground
U.S. Army Test and Evaluation Command
Yuma, AZ 85364
ATTN: Mr. Robert Faris

Commandant of the Marine Corps
Headquarters, Marine Corps
Washington, DC 20380
ATTN: Technical Library

Director, Development Center
Marine Corps Development and Education Command
Quantico, VA 22134
ATTN: Technical Library

NASA Ames Research Center
Moffett Field, CA
ATTN: Technical Library

NASA Langley Research Center
Langley Station
Hampton, VA
ATTN: Mr. L. Spearman
Mr. R. Shearer
Technical Library

Director, Defense Research and Engineering
Department of Defense
Washington, DC 20305
ATTN: Technical Library (2)

Advanced Research Projects Agency
Department of Defense
Washington, DC 20305
ATTN: Technical Library (2)

Defense Documentation Center
Cameron Station
Alexandria, VA 22314 (2)

DISTRIBUTION (Continued)

Local:

C	
C05	
D	
D1	
D2	
E	
E41	
F	
G	
G01	
G02	
G10	
G103	
G11	
G20	
G23	
G23 (Hill)	
G30	
G302	
G303	
G32	
G35	
G35 (Adams)	
G41 (Graff)	
G41 (Piper)	
K	
K20	
K204	
K21	
K21 (Moga)	(10)
X210	(2)
X211	(2)